International Journal of Nanomedicine

Dovepress
Taylor & Francis Group

Open Access Full Text Article

ORIGINAL RESEARCH

Intratracheal Instillation of Silver Nanoparticles to Rats Induces Mitochondrial Fission and Aortic Damage: Protective Effect of Sodium Selenite

Shan He[1,2,*], P Andy Li[3,*], Jing He[4], Zhizhong Wang[5], Xuexing Liang[1], Zhehao He[5], Shaobin Jia[6,*], Wanrui Ma[1,*]

[1]Department of General Medicine, The First Dongguan Affiliated Hospital, Guangdong Medical University, Dongguan, Guangdong, People's Republic of China; [2]School of Clinical Medicine at Ningxia Medical University, Yinchuan, Ningxia, People's Republic of China; [3]Department of Pharmaceutical Sciences, Biomanufacturing Research Institute and Technological Enterprise (BRITE), College of Health and Sciences, North Carolina Central University, Durham, North Carolina, USA; [4]Department of Geriatric and Special Medicine, General Hospital of Ningxia Medical University, Yinchuan, Ningxia, People's Republic of China; [5]Department of Epidemiology and Health Statistics, School of Public Health at Guangdong Medical University, Dongguan, Guangdong, People's Republic of China; [6]Heart Centre, General Hospital of Ningxia Medical University, Yinchuan, Ningxia, People's Republic of China

*These authors contributed equally to this work

Correspondence: Shaobin Jia; Wanrui Ma, Email jsbxn@163.com; mwr_1984stone@163.com

Purpose: This study aims to investigate the influence of AgNPs intratracheal instillation on mitochondrial fission in aortic endothelial cells of rats and to explore the therapeutic effects of sodium selenite (Se).

Animals and Methods: Male Sprague Dawley rats were divided into four groups (n=8): Control group (A), AgNPs exposure group (B), Se treated group (C), and Se+ AgNPs treated group (D). Rats in groups B and D received one dose of intratracheal instillation of AgNPs, while groups A and C received the same volume of 0.9% NaCl intratracheally. Rats in groups C and D were also intraperitoneally injected with sodium selenite for 7 days immediately after the AgNPs exposure. Morphological changes of the aorta were assessed using hematoxylin and eosin (HE) staining and electron microscopy. Masson's Trichrome Staining assayed collagen deposition in the aorta. Reactive oxygen species (ROS) generation, caspase-3 activity, and mitochondrial fission markers were analyzed.

Results: Exposure to AgNPs increased collagen deposition and caused ultrastructural damage to endothelial cells in the aorta, including reduction of cytosolic contents, dissolution of mitochondrial cristae, and swollen mitochondria. Levels of ROS and cleaved caspase-3 increased moderately in AgNPs group ($p<0.05$ vs Control). Mitochondrial fission markers Dynamin-related protein 1 (Drp1) and mitochondrial fission protein 1 (Fis1) in the aortic tissue homogenate of the AgNPs group nearly doubled the values of those in Control group ($p<0.05$ vs Control). Se alleviated AgNPs-induced ultrastructure changes and this effect was associated with suppressed ROS accumulation, inhibited caspase-3 activation, and attenuated mitochondrial fission.

Conclusion: This study demonstrates that AgNPs induced oxidative stress, caspase 3 activation, and mitochondrial fission are linked to the morphological alterations of the aortic endothelial cells; and these adverse effects resulted from AgNPs can be alleviated by sodium selenite, suggesting that selenite could be used as a protective agent against AgNPs toxicity.

Keywords: aorta, endothelial cells, mitochondrial fission, reactive oxygen species, selenium, silver nanoparticles

Introduction

The extensive utilization of silver nanoparticles (AgNPs) in medical (antimicrobial, drug delivery, biosensors for disease detection) and a range of industrial and environmental fields (food packaging, water purification, photovoltaics, etc.) raised attention to their adverse effects on human health.[1–4] However, due to their small sizes, they can easily enter the body through various routes (skin, inhalation, or ingestion) and become biotoxins by depositing in tissues and organs, which may induce various health outcomes.[5] Previous studies have shown that AgNPs deposit in various organs,[6] such as

Received: 7 March 2025
Accepted: 18 August 2025
Published: 23 September 2025

the lungs, spleen, liver, kidneys, thymus, and heart of SD rats after exposure.[7] The cardiovascular system represents an important route for the distribution, bioaccumulation, and bioavailability of different circulating substances in the bloodstream. Still, there are limited studies on the effect of AgNPs on the cardiovascular system,[8] more specifically on blood vessel endothelial cells. It has been demonstrated that AgNPs could induce injury and dysfunction of Human Umbilical Vein Endothelial Cells (HUVECs) by activating Inhibitor of Nuclear Factor kappa-B Kinase (IKK)/Nuclear Factor kappa-B (NF-κB) pathway, which may be an initiating factor for the development of atherosclerosis.[9] However, the toxic effect of AgNPs exposure on the aortic endothelial cells and the possible mechanism are unclear.

Mitochondria, crucial subcellular organelles that control cellular energy metabolism, undergo fission and fusion constantly. This process is termed "mitochondrial dynamics".[10] The dynamic behavior of mitochondria helps cells adapting to various stressors and maintain normal physiological functions.[11] Mitochondrial fission, the division of one mitochondrion into two daughter mitochondria, is mainly regulated by two key proteins: Fission 1 (Fis1) and dynamin-related protein 1 (Drp1).[12] Normal mitochondrial fission helps to remove mitochondrial metabolic wastes. Reduced fission may cause accumulation of denatured proteins and metabolic wastes in the cell, eventually cause cell dysfunction and death. However, excessive fission also reduces ATP production, increases ROS production, and even affects the integrity of mitochondrial structure.[13] Mitochondrial fission as a biomarker of endothelial dysfunction and atherosclerosis has been reported by previous studies that demonstrated a link between disruption of mitochondrial dynamics and human disease, including cardiovascular diseases and cellular senescence.[14,15] Inhibition of Drp1 has been shown to ameliorate endothelial dysfunction and suppress atherosclerosis in apolipoprotein E knockout diabetic mice, suggesting a potential therapeutic approach for treating macrovascular complications in diabetic patients.[16]

It has been reported that AgNPs cause mitochondrial dynamic imbalance in rat liver through increasing permeability of the mitochondrial membrane, and inhibit the electron transport chain, which in turn leads to ROS generation and oxidative stress.[17] Our published data demonstrated that intratracheal instillation of AgNPs to rats results in excessive mitochondrial fission and/or inhibition of mitochondrial fusion in the lung and heart tissues.[18,19] Therefore, mitochondrial dynamic imbalance may play an important role in mediating the cytotoxicity of AgNPs in the heart and lungs, while the effects of AgNPs on aortic endothelial cells remain to be studied.

Selenium is an essential micronutrient for human health, providing anti-inflammatory, anti-oxidative, and immune system enhancement properties.[20] Although selenium is recognized as a heavy metal antioxidant, the evidence that selenium against the toxicity of nano-heavy metals, including AgNPs, is limited. AgNPs induce hepatotoxicity through increasing heat shock protein 60 (HSP60),[21] and the overexpression of HSP60 is associated with selenium deficit.[22] One study found that supplementation of selenium reduced AgNPs-induced hepatotoxicity.[23] Further, selenium can prevent AgNPs-induced oxidative stress, caspase-3 activation, mitochondrial dynamic imbalance, mitophagy, and preserving pulmonary and cardiac structural and functional integrities.[18,19] The Current study aims to investigate whether AgNPs cause mitochondrial dynamic imbalance, morphological and functional alterations in rat aortic endothelial cells, and whether sodium selenite is capable of counteracting the induced alterations therapeutically.

Materials and Methods

Nanoparticle Preparation and Characterization

Silver nanoparticles (specific type, US Research Nanomaterials, USA) were dissolved in ddH2O containing 1 mg/mL of AgNPs and 1% DMSO). The nanoparticles were kept in a dark and iced-water bath and sonicated for at least 30 minutes prior to being used for animal to ensure uniform dispersion. The size and physicochemical properties of the nanoparticles were characterized in our previous publication and in the current study.

Animals and Treatment

Thirty-two Male Sprague Dawley rats, aged 6–8 weeks, with an average weight of 200±20g were selected. The rats were fed standard laboratory rat chow for an acclimatization period of 7 days in a temperature-controlled room (24°C±4°C) with a 12-hour light/dark cycle and 50%±20% humidity. All animal surgical procedures were conducted in strict accordance with the Guidelines for Laboratory Animal Care and Use issued by Chinese National Guidelines (GB/T

35892-20,181) 2018 and were approved by the Institutional Review Board of the General Hospital of Ningxia Medical University (approval numbers 2016–089).

The animal groups and treatment information is given in Figure 1. The rats were randomly divided into four groups (n=8 in each): A, Control group; B, AgNPs exposure group; C, Se treated group; and D, Se + AgNPs treated group. The AgNPs exposure groups (B and D) received an intratracheal instillation (IT) of the AgNPs stock suspension (1 mg/kg, 200 μL/rat) followed by 100 μL of air. The Control and Se treated groups (A and C) received a similar volume of 0.9% NaCl by intratracheal instillation. Groups C and D were intraperitoneally (IP) injected with sodium selenite (0.2 mg/kg) concomitantly with AgNPs IT and repeated once daily for 7 days. The dose selections for AgNP and selenite were based on our previous studies.[18,19] The animals in Groups were i.p. injected with 0.9% normal saline once daily for 7 days. After 21 days of initial AgNPs and/or selenite injection, the aortae were dissected from each rat under anesthesia with an intraperitoneal injection of chloral hydrate (4%) and washed three times in an ice-cold saline solution immediately. Then, the aortic tissues were cut into four parts for further processes. One part of the tissue was fixed with a 4% paraformaldehyde solution for histo-pathological examinations. The second part was placed in 2% glutaraldehyde for electron

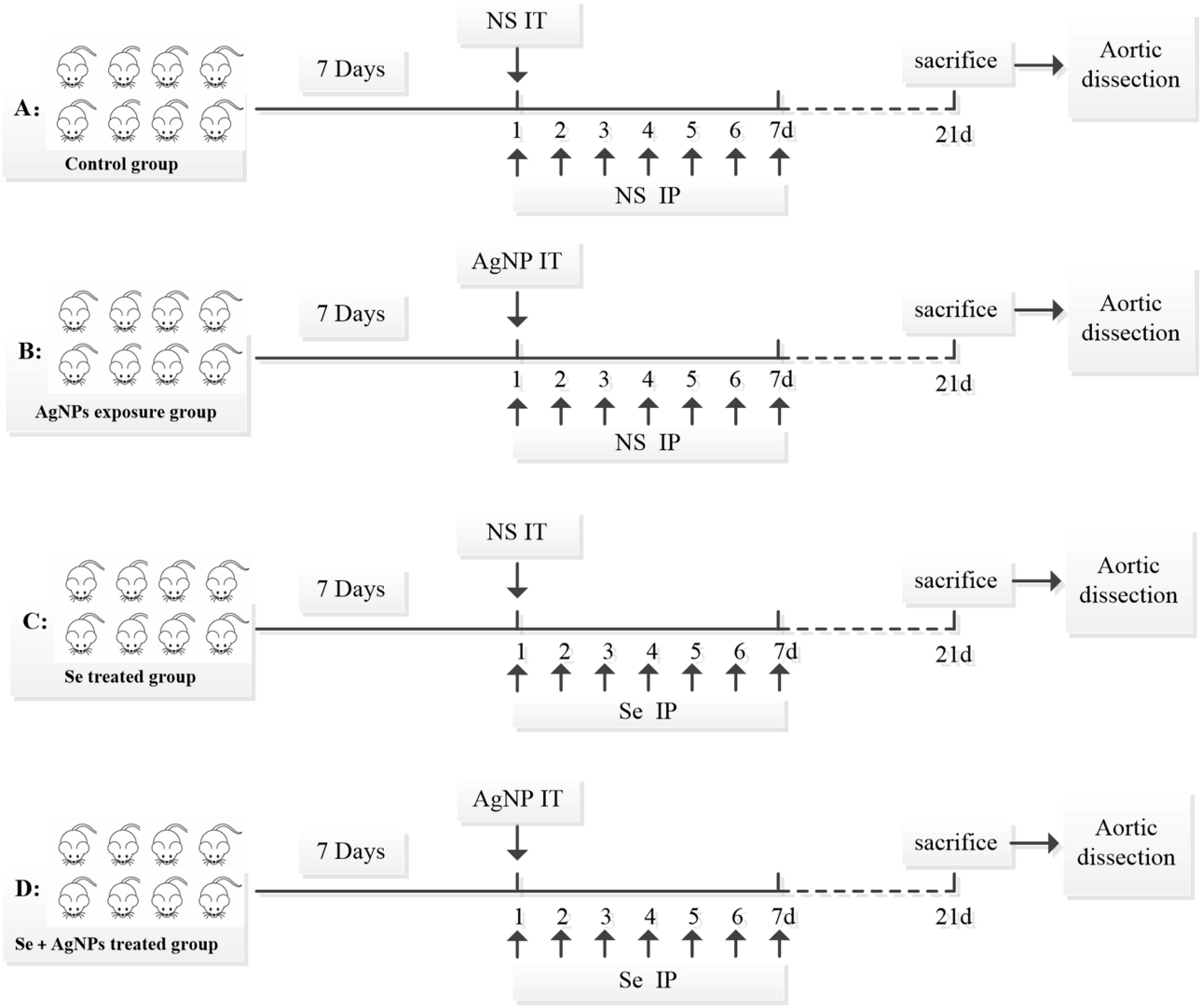

Figure 1 The design of animal experiments and treatment. Rats were randomly allocated into four groups (n=8/group): (**A**) Control group, (**B**) AgNPs exposure group, (**C**) Se treated group, and (**D**) Se + AgNPs treated group. The rats were treated with a single intratracheal instillation (IT) of the AgNPs stock suspension (1 mg/kg, 200 μL/rat) or a similar volume of 0.9% NaCl. The intraperitoneal injection of sodium selenite (0.2 mg/kg) or NS (1 mL) was administered once daily for 7 days immediately after the AgNPs intratracheal instillation. The aortae were dissected following the sacrifice of rats on the 21st day after intratracheal instillation.
Abbreviations: AgNPs, silver nanoparticles; IP, intraperitoneal injection; NS, normal saline; Se, sodium selenite.

https://doi.org/10.2147/IJN.S524020

microscope study. The third part was fixed in the frozen embedding agent OCT for immunohistochemistry. The fourth part was frozen in liquid nitrogen and stored in the −80 °C refrigerator for subsequent protein assays.

Histopathological Examinations

For histological examination, the collected aortic segment was fixed with a 4% paraformaldehyde solution for 48 hours, dehydrated in ascending concentrations of ethanol, cleared with xylene, and embedded in paraffin. Five-micrometer-thick sections were cut from the paraffin blocks and stained with hematoxylin and eosin. The extent of collagen fibrosis was detected using Masson's Trichrome Stain Kit from Solarbio (G1340) following the manufacturer's protocol. A histopathologist (S.A)., who was blinded to the grouping information, assessed the stained sections under a light microscope (OLYMPUS BX43, Tokyo, Japan). The Image J analysis software was used to determine the areas of blue-stained collagen and aortic media in each section, and the ratio of collagen area to aortic media area was used to represent collagen content.

Transmission Electron Microscopy Study

The aortic tissues were fixed in 2% glutaraldehyde for 2 hours at 4°C, then washed three times with 0.1M dimethyl sodium arsenate at 2-hour intervals, followed by post-fixation in 4% osmic acid for 2 hours and two washes in 0.1M dimethyl sodium arsenate. The tissues were then dehydrated in a graded series of ethanol and embedded in epoxy resin. The resin was polymerized for 48 hours at 60°C. Ultrathin sections were cut from the blocks and stained with uranyl acetate and lead citrate. The sections were mounted on copper grids, and observations were carried out and images were captured using a transmission electron microscope (Hitachi H-7650, Tokyo, Japan).

ROS Detection

The concentration of ROS was measured using the fluorescent probe BBoxi O13 follow the instructions of the ROS frozen section test kit. Briefly, cleaning solution (50 μL) was added to the tissue sections for 5 minutes. Then, a fluorescence probe working solution (50μL) was added on each section (the ratio of BBoxiProbeO13 active oxygen fluorescence probe to pure water was 1:150), and incubated in a wet box in a 37°C incubator. After 20 min of incubation, the sections were rinsed 3 times with PBS. The fluorescence intensity, which detects the ROS signal, was measured at an excitation wavelength of 340–380 nm and the signal intensity was analyzed using program in a fluorescence microscope (OLYMPUS BX43).

Immunofluorescence

Immunofluorescence detection of cleaved-Caspase 3 was performed with 4-μm paraffin cross-sections from the aorta of rat. Paraffin sections were dewaxed routinely and placed in a 0.01M citrate buffer solution (pH = 6.0) for 5 minutes in a hot water bath to unmask the antigens. Endogenous peroxidase activity was quenched by incubating the slides in methanol/water (1:1) containing 0.3% hydrogen peroxide. To block nonspecific binding sites, 30% goat serum was applied at room temperature for 30 minutes. The slides were then incubated overnight at 4 °C with Cleaved-Caspase 3 primary antibody (1:500, ab49822, Abcam) and subsequently washed to remove excess primary antibody. Next day, the slides were incubated with a goat anti-rabbit secondary antibody for one hour, followed by washing to remove excess secondary antibody. The nuclei were stained with DAPI, and the slides were immediately observed under a fluorescence microscope (OLYMPUS BX43) and images were captured. The fluorescence intensity in the images was quantified using Image Pro Plus software.

Western Blot

The aortic artery tissues were homogenized using the total protein extraction kit from KeyGEN BioTECH (KGP2100) according to the manufacturer's instructions. The homogenates were centrifuged at 1000×g for 10 minutes to separate the supernatant from the pellet. The supernatant containing the whole protein was collected, and lysed in an ice-water bath. The protein concentrations were measured using the BCA Protein Assay Kit (KeyGEN BioTECH). Equal amounts of protein were loaded onto an SDS-PAGE gel for electrophoresis. The proteins on the gel were transferred onto

nitrocellulose membranes (Invitrogen) and blocked with 10% skim milk for 1 hour to reduce nonspecific protein binding. The blots were then incubated with primary antibodies against Drp1 (1:1000, ab184247, Abcam), Fis1 (1:1000, GTX111010, Gene Tex), and GAPDH (1:1000, sc-1616, Santa Cruz Biotechnology, CA, USA) overnight at 4°C. The membranes were washed and incubated with horseradish peroxidase-labeled secondary antibodies (specify type) at room temperature for 1 hour. The protein bands were visualized using the Pierce ECL Western Blotting Substrate. The bands of the control protein GAPDH were used to normalize the expression levels of the targeted proteins, then the ratios of the targeted protein bands and loading control were calculated.

Statistical Analysis

We used SPSS version 22.0 (Chicago, IL, USA) for statistical analysis. Each experiment was repeated three times, and data are presented as mean ± standard deviation (x ± s). We used the One-Way ANOVA test and post hoc comparisons between groups (exact binomial 95% confidence intervals [CIs]). P values < 0.05 is considered as statistically significant.

Results

Characterization of Silver Nanoparticles

TEM and DLS were used to characterize the morphologies and sizes of AgNP in the working solution as shown in Figure 2. The TEM results showed that the AgNPs were mostly spherical, and ranged in size from 15 to 35 nm, with a mean size of 24.67 ± 5.28 nm (Figure 2A and B). As shown in Figure 2C, the hydrodynamic diameter of the AgNPs in

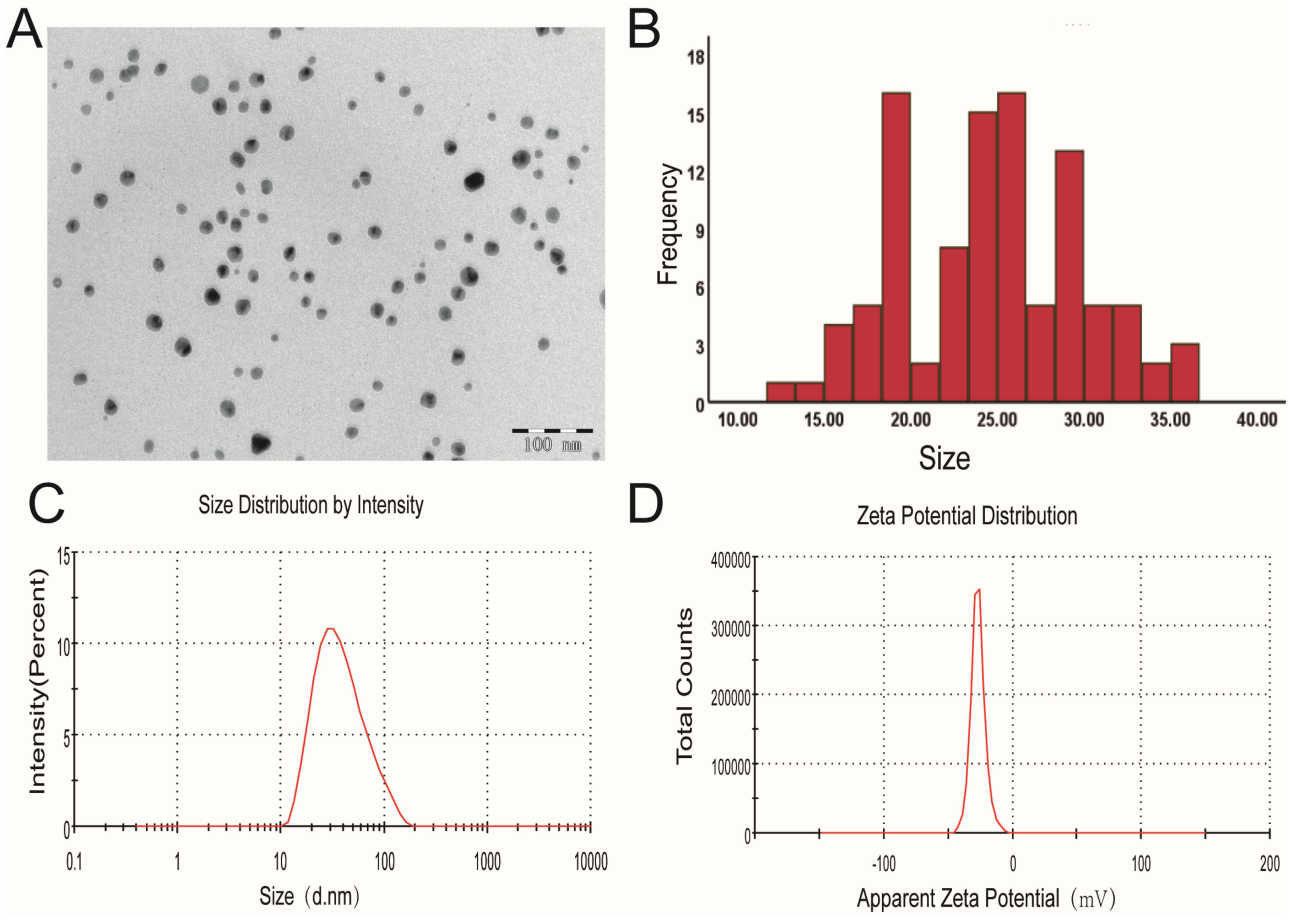

Figure 2 Characterization of AgNPs. (**A**) Representative TEM image of AgNPs. TEM magnification ×30,000. Scale bars: 100 nm. (**B**) Quantification of AgNPs analysis. (**C**) Size distribution of AgNPs in NS. (**D**) Zeta potential of AgNPs in NS.
Abbreviations: AgNPs, silver nanoparticles; NS, normal saline.

https://doi.org/10.2147/IJN.S524020

1% DMSO ddH2O measured by DLS was 38.6 ± 6.43 nm. The zeta potentials were −24.9 ± 1.65 mV in 1% DMSO ddH2O (Figure 2D). The results showed that AgNPs have strong stability and low aggregation resistance in 1% DMSO ddH2O due to their high negative zeta potential.

AgNPs Increased the Contents of Smooth Muscle and Collagen

Histopathological Examination was performed and the results were shown in Figure 3A. There was no significant difference in the aortic tissue sections among the four groups observed by optical microscope. As shown in Figure 3A, endocardial cells, elastic fibers, and smooth muscles were presented clearly. The aortic intima was thin and uniform with a smooth surface, and the endothelial cells were flat and regular, arranged neatly without thickening. Vascular smooth muscle cells were long, spindle-shaped, arranged regularly, and had uniform nuclei. Masson staining was then conducted to assess collagen deposition in the aortic tissue. Vascular smooth muscle cells and elastic fibers appeared red while interstitial collagen fibers were blue in the rat aorta (Figure 3B). The collagen volume fraction (percentage of the collagen positive blue area to the total tissue area) was analyzed using Image J software. After AgNPs exposure, the contents of smooth muscle and collagen in the aorta was 9.75±0.95 and 20.25±12.79 in control and Se treated group, respectively. Intratracheal instillation of AgNPs increased the contents of smooth muscle and collagen to 73.25±13.18 ($P<0.05$ vs Control), while these abnormalities reverted to normal status in Se+AgNPs co-treated groups (Figure 3C).

AgNPs Resulted in Ultrastructural Alterations of the Aortic Endothelial Cells

The ultrastructural changes in endothelial cells of aortic tissue were observed by TEM. Aortic endothelial cells were flat with homogeneous nuclear chromatin in both the control and selenium (Se) groups as shown in Figure 4a and c, respectively. Meanwhile, tight attachment between aortic endothelial cells and the endothelium was observed. In AgNPs group, the breakdown of endothelial cell membrane and nuclear envelope (yellow arrow in Figure 4b1) were observed, and cytoplasmic vacuolation (orange arrows in Figure 4b2) were apparent. However, there were no obvious abnormalities in the ultrastructure of the endothelial cells in Se+AgNPs group (Figure 4d) compared with the AgNPs group.

Given the importance of mitochondria in cellular function and survival, the ultrastructural changes of mitochondria were further examined by TEM. The mitochondrial structures in the normal control group and Se control group were intact, with clear cristae and normal size (blue arrows in Figure 4A and C). After AgNPs exposure, remarkable changes in mitochondria occurred with the disappearance of the bilayer membrane, deformed with swelling, and cristae dissolution (green arrow in Figure 4B1). Silver nanoparticles (red arrows in Figure 4B1 and B2) were found within the nucleus. In the Se treatment group (Figure 4D), the AgNPs-caused ultrastructural alterations (mitochondrial swelling and cristae dissolution) were prevented. Unlike AgNPs group, the silver particle accumulation and cell membrane disappearance were not found in the Se+AgNPs co-treated group.

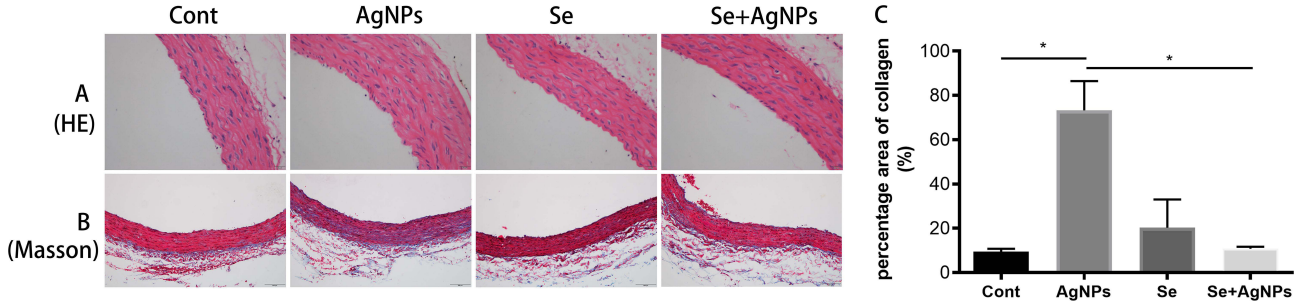

Figure 3 Assessment of aorta by H&E and Masson staining. (**A**) H&E stain shows the structure of the aorta. Scale bar = 20μm. (**B**) Effects of AgNPs on the aortic collagen deposition and morphometry. The representative photomicrographs of Masson's trichrome-stained aortic section. (**C**) The summarized bar graph showing the contents of smooth muscle and collagen in the aorta.

Notes: The Data were collected from three independent images and presented as means ± SD. *p<0.05 were considered to be statistically significant.

Abbreviations: Cont, control; AgNPs, silver nanoparticles; Se, selenite; H&E, hematoxylin and eosin; SD, standard deviation.

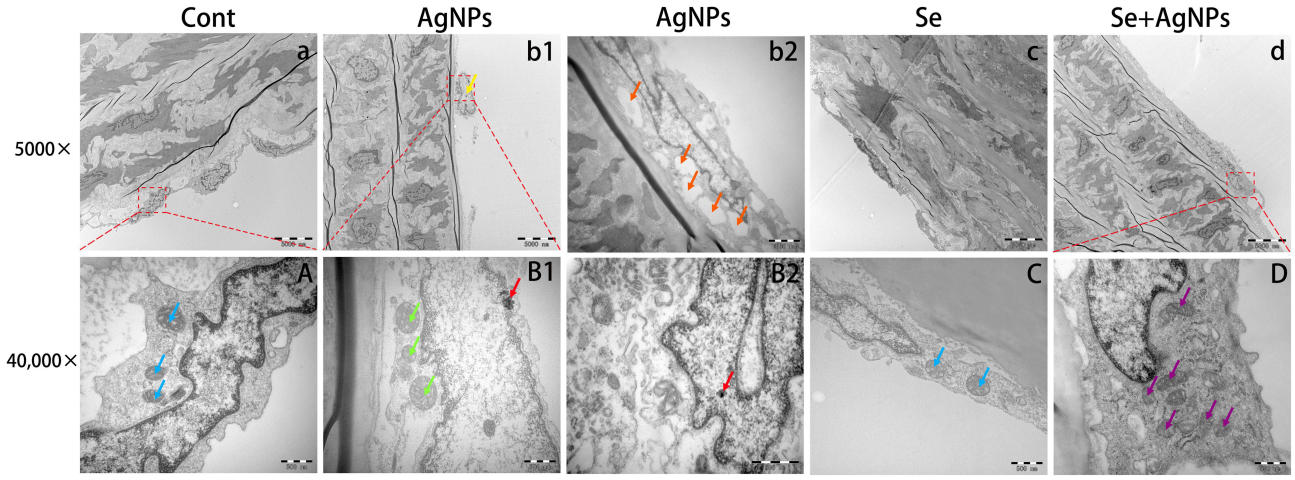

Figure 4 Effects of AgNP on the endothelial cell ultrastructure of aortic tissue. (I) Representative TEM images of ultrastructural changes in the aortic tissue sections. (a-d) Zoomed-in TEM image at 5000×. (II) (A–D) Representative TEM images of ultrastructural changes in the endothelial cell. Zoomed-in TEM image at 40,000×. yellow arrow, nucleus; Orange arrow, cytoplasmic vacuolation; blue arrow, normal mitochondria; red arrow, AgNPs within the nuclei; green arrow, damaged mitochondrial; purple arrows, basically normal mitochondria;.
Abbreviations: Cont, control; AgNPs, silver nanoparticles; Se, selenite.

AgNPs Increased Oxidative Stress

The ROS fluorescent probe was used to detect the amount of ROS in the frozen sections of the aorta, and the fluorescence intensity was analyzed by Image J software. As shown in Figure 5A, the AgNPs-treated group exhibited a significant increase in the production of ROS compared to the control group ($P<0.05$). After the addition of sodium selenite, the production of ROS was significantly reduced compared with the AgNP group ($P<0.05$). A summarized bar graph is given in Figure 5B.

AgNPs Activated Caspase-3

Apoptosis was detected using cleaved caspase-3 antibody, which is a biomarker for apoptosis. As shown in Figure 6, occasional scattered caspase-3 positively stained cells were observed in the Control group. After intratracheal instillation of AgNPs, the number of caspase-3 positive cells significantly increased (1.079 ± 0.04 vs 1.0). Se+AgNPs treated group reduced caspase-3 positively stained cells to control level. A set of representative images is given in Figure 6A and a summarized bar graph in Figure 6B.

AgNPs Shifted the Mitochondrial Dynamics Toward Fission

Mitochondrial fission markers, Drp1 and Fis1, were detected using Western blots. As showed in Figure 7, AgNPs treatment increased the protein levels of Drp1 and Fis1 in the aorta ($P<0.05$), suggesting an increase in mitochondrial fission. In contrast, treatment with sodium selenite significantly decreased the levels of Drp1 and Fis1 in the AgNPs+Se group compared to the AgNPs group, suggesting that sodium selenite ameliorated AgNPs-induced mitochondrial fission.

Discussion

The present study has demonstrated that AgNPs increased collagen deposition and caused ultrastructural damage to the endothelial cells of the aorta. In addition, AgNPs led to mitochondrial swelling, ROS production, caspase-3 activation, along with elevated levels of mitochondrial fission markers, Drp1 and Fis1. Treatment with sodium selenite alleviated AgNPs-induced ultrastructural alterations, oxidative stress, caspase-3 activation, and mitochondrial fission.

The major routes of AgNPs exposure include inhalation, ingestion, dermal contact, and direct entry into systemic circulation via intraperitoneal (i.p.) or intravenous (i.v.) injection, with inhalation being one of the primary methods of exposure. The common methods for animal inhalation modeling include whole-body exposure inhalation, nebulized

https://doi.org/10.2147/IJN.S524020

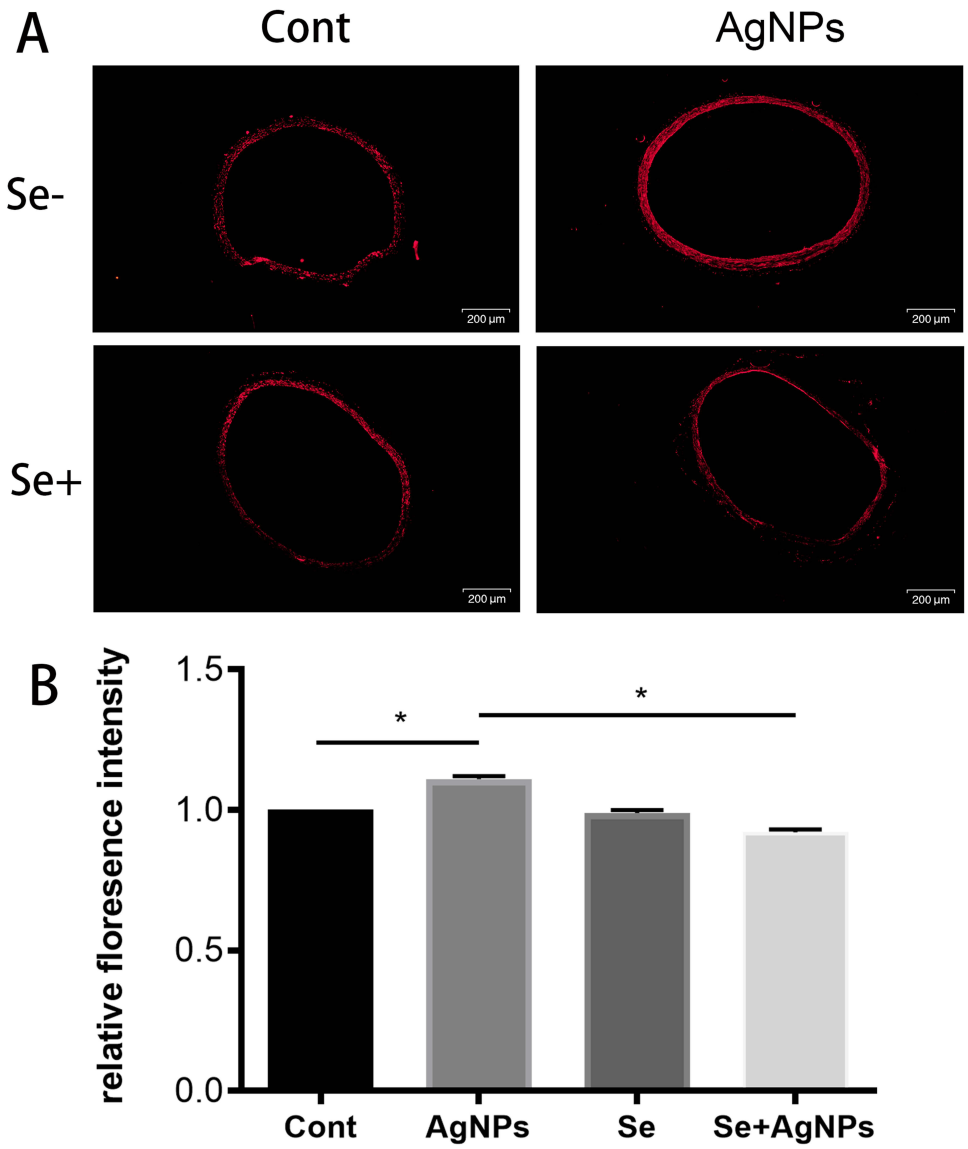

Figure 5 Assessment of ROS in aorta. (**A**) Intracellular ROS levels were measured using fluorescent probes BBoxi O13, Representative microscopic images of ROS in aorta. (**B**) The bar diagrams present their relative expression. The experiment was repeated three times for analysis.
Notes: The data represent means ± SD. Scale bar = 200 μm. *p<0.05.
Abbreviations: Cont, control; AgNPs, silver nanoparticles; Se, selenite; SD, standard deviation.

inhalation, nasal drip, or intratracheal instillation. Since the first two methods require special exposure chambers and are more expensive, intratracheal instillation was chosen.

Epidemiological evidence has shown that exposure to metal nanoparticles is strongly linked to cardiovascular damage and, consequently, increases the risk of cardiovascular morbidity and mortality.[24,25] Vascular endothelial cell injury plays an important role in the initiation and development of cardiovascular diseases. AgNPs intratracheal instillation to rats causes inflammatory responses, resulting in reduced coronary reactivity.[26] However, the impact of AgNPs on vascular endothelial cells is complex and remains unclear. In our study, AgNPs accumulation was found within the endothelial nucleus, which is consistent with previous research showing that the agglomerates of AgNPs were observed on the endothelial cell membrane as well as inside the cells using atomic force spectroscopy.[27] Although no obvious abnormalities were observed in aortic tissue sections that were stained with Hematoxylin and eosin in AgNPs and/or selenite-treated animals, Masson's trichrome staining revealed that AgNPs increased collagen deposition and caused ultrastructural impairment as reflected by the cytoplasmic vacuolation, reduction of cytosolic contents and subcellular organelles,

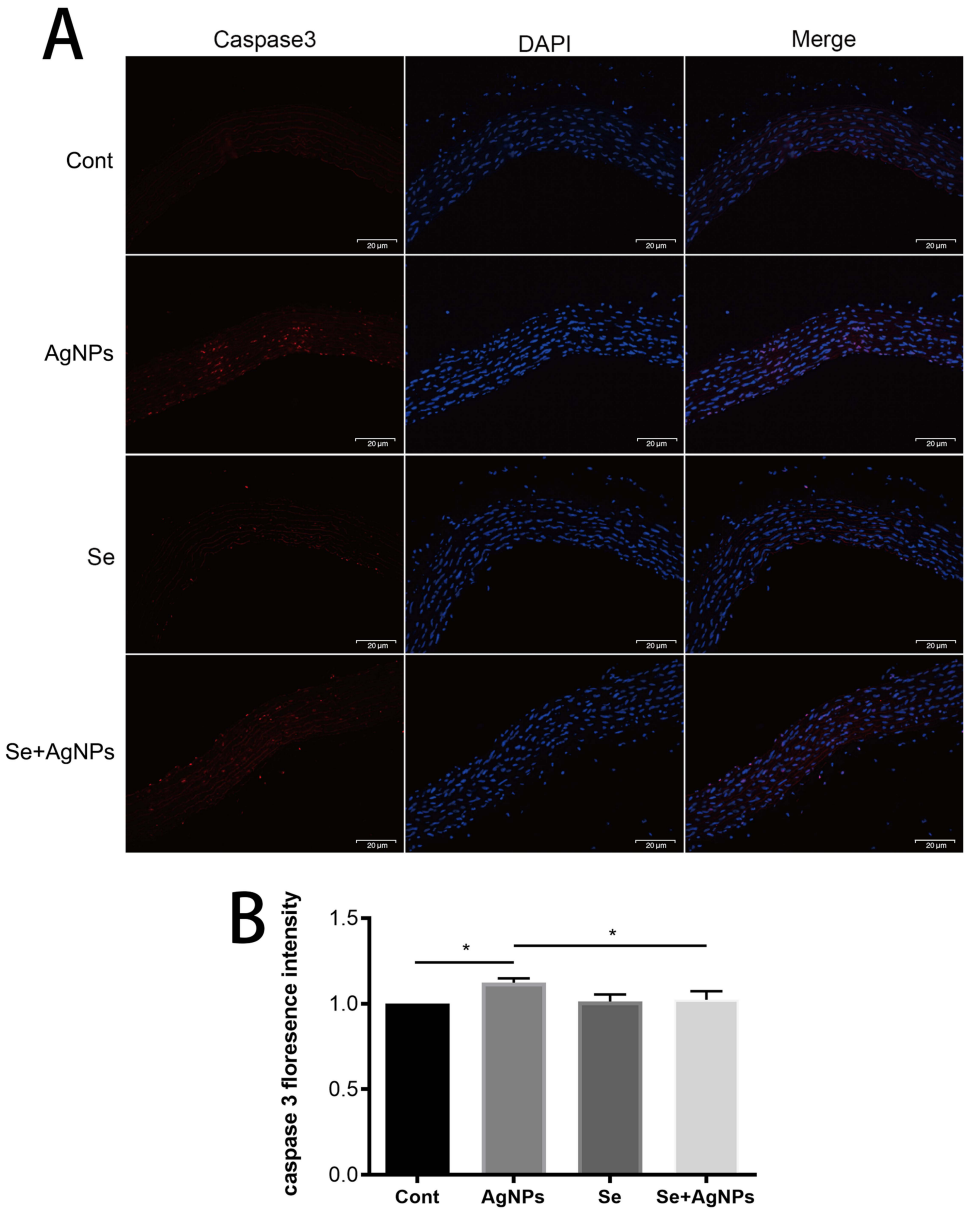

Figure 6 AgNPs actives caspase-3.(**A**) The representative Immunofluorescence photomicrographs showing expression of caspase3 proteins. Original magnification is 200×. (**B**) The bar diagrams present their relative expression.
Notes: The data represent means ± SD. Scale bar = 20 μm.*p<0.05.
Abbreviations: Cont, control; AgNPs, silver nanoparticles; Se, selenite; SD, standard deviation.

swollen mitochondria, and loss of mitochondrial cristae, with disappearing of mitochondrial bilayer membrane. Administration of sodium selenite attenuated the above AgNPs-induced ultrastructural alterations of the aortic endothelial. Although we have characterized the physical property of the AgNPs using TEM and DLS (Figure 2) and presented the deposition of AgNPs in the endothelial cells of the aorta in Figure 4, the pharmacokinetic or biodistribution data were not provided to confirm that AgNPs reach the aortic endothelium throughout the body. We plan to address this limitation by investigating the pharmacokinetic profile and tissue distribution of AgNPs in future studies.

Both in vitro and in vivo experiments have shown that oxidative stress is one of the vital mechanisms associated with the cytotoxicity of the AgNPs.[28–30] Various cell lines, including HUVECs, have been used to elucidate the impact of AgNPs on oxidative stress.[9,31] Their results demonstrated that AgNPs entered and sited inside the HUVECs, where increased ROS production was detected.[32] In current experiments using frozen sections of the aorta, we detected

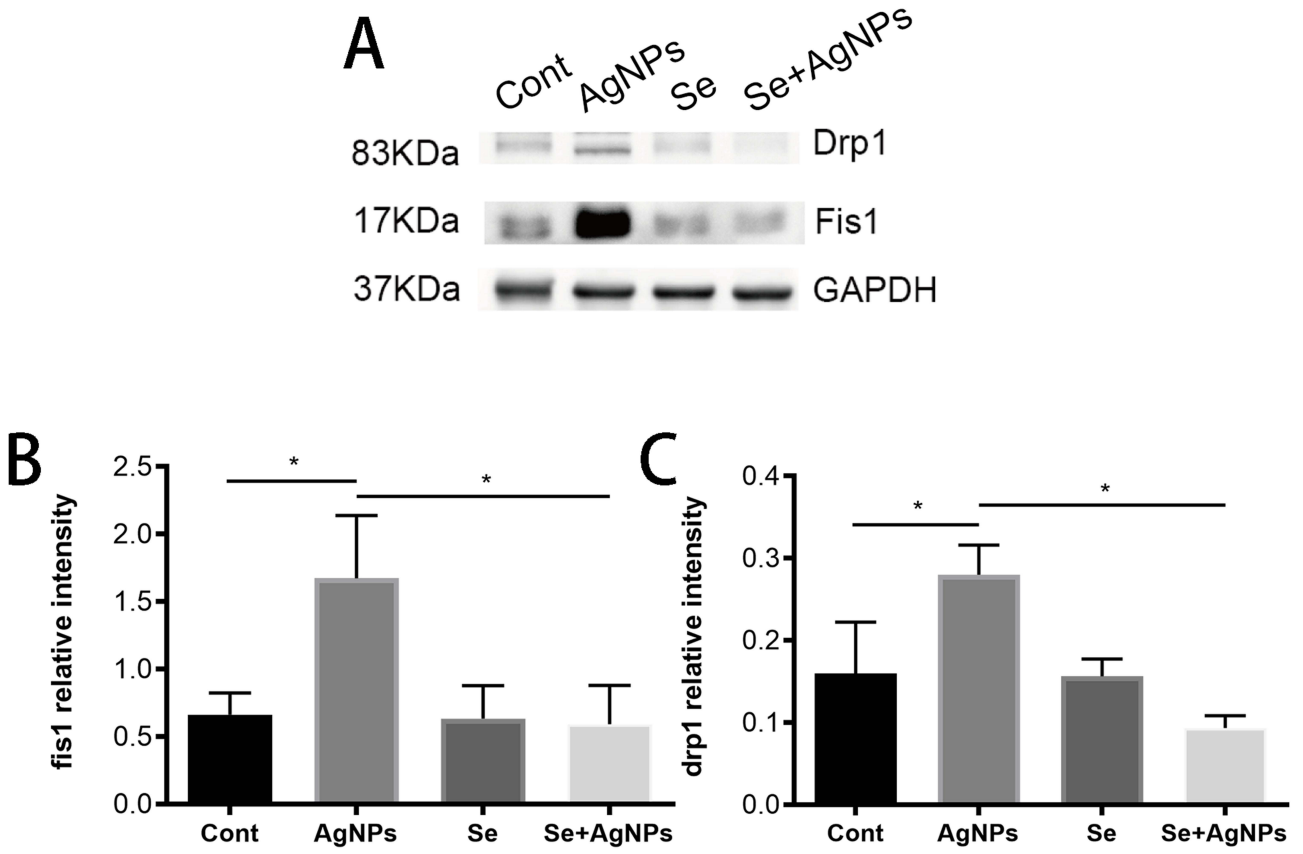

Figure 7 AgNPs induces mitochondrial dynamic imbalance towards fission. (**A**) The representative Western blot of mitochondrial fission protein Drp1 and Fis1 expression in rat. (**B–C**) Levels of these proteins expression were normalized to GAPDH. Band intensities were quantified using Image J software.
Notes: The data represent means ± SD. *p<0.05.
Abbreviations: Cont, control; AgNPs, silver nanoparticles; Se, selenite; SD, standard deviation.

increased amount of ROS in the aortic endothelial cells of AgNPs treated animals, which is consistent with previous studies.[9,31–33] It has been reported that AgNPs deplete antioxidant molecules, inhibit mitochondrial electron transport chain, and alter enzymatic production of reactive oxygen species.[30,31] Mitochondria are also the major target of oxidative stress and the initiator of several apoptotic cell death pathways.[34] Activation of apoptosis involves a cascade of proteases, among them, caspase 3 is considered as a cell death executioner. As expected, immunofluorescent staining of cleaved caspase-3 unveiled an increased number of cleaved caspase-3 positive cells in the AgNPs group, suggesting that AgNPs exposure activated the caspase-3 dependent cell death pathway. Caspase-3 positively stained cells return to normal seven days after the Se co-treated. Therefore, selenite can alleviate AgNPs-induced apoptosis through decreasing caspase-3 activation. Selenite is an anion containing selenium in the +4-oxidation state, and selenite-based compounds play various roles in acting as antioxidants, participating in enzyme activities, and regulating cell functions. The current study demonstrated that it can neutralize the ROS generated by AgNPs, which may be a factor in caspase-3 activation, thereby inhibiting the overall process of apoptosis.

Mitochondria are highly dynamic organelles undergoing continuous events of fission and fusion, which play an indispensable role in many cellular processes.[10] Either increased or decreased mitochondrial fission can lead to disease conditions. Previous studies have demonstrated that increased ROS induces Drp1-and mitochondrial fission.[35–37] Consistent with current findings that AgNPs exposure increased the generation of ROS and activated cleaved caspase 3, we have also found that mitochondrial fission proteins Drp1 and Fis1 are significantly increased after AgNPs instillation. Compared with the AgNPs group, Se-AgNPs co-treatment prevented the elevations of mitochondrial fission markers Drp1 and Fis1, suggesting selenite can block AgNPs-induced mitochondrial fission. Unfortunately, we were unable to test the dose-response effect and establish causal inference; future studies are needed to confirm these findings.

Conclusion

Our data demonstrate that exposure to AgNPs increases collagen deposition, nuclear abnormalities, mitochondrial swelling, and the dissolution of mitochondrial cristae. Further, AgNPs enhanced ROS production, caspase-3 activation, and mitochondrial fission markers. Treatment with sodium selenite may alleviate the morphological alterations associated with inhibiting ROS formation, caspase-3 activation, and mitochondrial fission.

Author Contributions

All authors made a significant contribution to the work reported, whether that is in the conception, study design, execution, acquisition of data, analysis and interpretation, or in all these areas; took part in drafting, revising or critically reviewing the article; gave final approval of the version to be published; have agreed on the journal to which the article has been submitted; and agree to be accountable for all aspects of the work.

Funding

The authors acknowledge the financial support from the Dongguan Science and Technology of Social Development Program (Grant No. 20231800940182), the Talent Development Foundation of The First Dongguan Affiliated Hospital of Guangdong Medical University (Grant No. GCC2023003), the Dongguan Outstanding Young Medical Talent Recruitment and Training Program, and the National Natural Science Foundation of China (Grant No. 82060057).

Disclosure

The authors report no conflicts of interest in this work.

References

1. Lee SH, Jun BH. Silver nanoparticles: synthesis and application for nanomedicine. *Int J Mol Sci*. 2019;20(4):865. doi:10.3390/ijms20040865
2. Yin Zhang J, Zhao IS, Zhao IS, et al. The antibacterial mechanism of silver nanoparticles and its application in dentistry. *Int J Nanomed*. 2020;15:2555–2562. doi:10.2147/IJN.S246764
3. Wang H, Yan A, Liu Z, et al. Deciphering molecular mechanism of silver by integrated omic approaches enables enhancing its antimicrobial efficacy in E. coli. *PLoS Biol*. 2019;17(6):e3000292. doi:10.1371/journal.pbio.3000292
4. Burdușel AC, Gherasim O, Grumezescu AM, et al. Biomedical applications of silver nanoparticles: an up-to-date overview. *Nanomaterials*. 2018;8(9):681. doi:10.3390/nano8090681
5. Rezvani E, Rafferty A, McGuinness C, et al. Adverse effects of nanosilver on human health and the environment. *Acta Biomater*. 2019;94:145–159. doi:10.1016/j.actbio.2019.05.042
6. Hadrup N, Sharma AK, Jacobsen NR, et al. Distribution, metabolism, excretion, and toxicity of implanted silver: a review. *Drug Chem Toxicol*. 2022;45(5):2388–2397. doi:10.1080/01480545.2021.1950167
7. Wen HR, Dan M, Yang Y, et al. Acute toxicity and genotoxicity of silver nanoparticle in rats. *PLoS One*. 2017;12(9):e0185554. doi:10.1371/journal.pone.0185554
8. Gonzalez C, Rosas-Hernandez H, Ramirez-Lee MA, et al. Role of silver nanoparticles (AgNPs) on the cardiovascular system. *Arch Toxicol*. 2016;90(3):493–511. doi:10.1007/s00204-014-1447-8
9. Shi JP, Sun X, Lin Y, et al. Endothelial cell injury and dysfunction induced by silver nanoparticles through oxidative stress via IKK/NF-κB pathways. *Biomaterials*. 2014;35(24):6657–6666. doi:10.1016/j.biomaterials.2014.04.093
10. Tilokani L, Nagashima S, Paupe V, et al. Mitochondrial dynamics: overview of molecular mechanisms. *Essays Biochem*. 2018;62(3):341–360. doi:10.1042/EBC20170104
11. Chan DC. Mitochondrial dynamics and its involvement in disease. *Annu Rev Pathol*. 2020;15(1):235–259. doi:10.1146/annurev-pathmechdis-012419-032711
12. Sorrentino V, Menzies KJ, Auwerx J. Repairing mitochondrial dysfunction in disease. *Annu Rev Pharmacol Toxicol*. 2018;58(1):353–389. doi:10.1146/annurev-pharmtox-010716-104908
13. Yang J, Guo W, Wang J, et al. T-2 toxin-induced oxidative stress leads to imbalance of mitochondrial fission and fusion to activate cellular apoptosis in the human liver 7702 cell line. *Toxins*. 2020;12(1):43. doi:10.3390/toxins12010043
14. Adebayo M, Singh S, Singh AP, et al. Mitochondrial fusion and fission: the fine-tune balance for cellular homeostasis. *FASEB J*. 2021;35(6):e21620. doi:10.1096/fj.202100067R
15. Vasileiou PVS, Evangelou K, Vlasis K, et al. Mitochondrial homeostasis and cellular senescence. *Cells*. 2019;8(7):686. doi:10.3390/cells8070686
16. Wang QL, Zhang M, Torres G, et al. Metformin suppresses diabetes-accelerated atherosclerosis via the inhibition of Drp1-mediated mitochondrial fission. *Diabetes*. 2017;66(1):193–205. doi:10.2337/db16-0915
17. Teodoro JS, Silva R, Varela AT, et al. Low-dose, subchronic exposure to silver nanoparticles causes mitochondrial alterations in sprague-dawley rats. *Nanomedicine*. 2016;11(11):1359–1375. doi:10.2217/nnm-2016-0049
18. Ma W, He S, Xu Y, et al. Ameliorative effect of sodium selenite on silver nanoparticles-induced myocardiocyte structural alterations in rats. *Int J Nanomed*. 2020;15:8281–8292. doi:10.2147/IJN.S271457

19. Ma W, He S, Ma H, et al. Silver nanoparticle exposure causes pulmonary structural damage and mitochondrial dynamic imbalance in the rat: protective effects of sodium selenite. *Int J Nanomed*. 2020;15:633–645. doi:10.2147/IJN.S232986
20. Rayman MP. Selenium and human health. *Lancet*. 2012;379(9822):1256–1268. doi:10.1016/S0140-6736(11)61452-9
21. Shipelin VA, Kudan PV, Zgoda VG, et al. Effect of silver nanoparticles on protein composition of rat liver microsomal fraction. *Bull Exp Biol Med*. 2018;166(1):80–85. doi:10.1007/s10517-018-4293-5
22. Liu TQ, Yang TS, Pan TR, et al. Effect of low-selenium/high-fat diet on pig peripheral blood lymphocytes: perspectives from selenoproteins, heat shock proteins, and cytokines. *Biol Trace Elem Res*. 2018;183(1):102–113. doi:10.1007/s12011-017-1122-z
23. Ansar S, Alshehri SM, Abudawood M, et al. Antioxidant and hepatoprotective role of selenium against silver nanoparticles. *Int J Nanomed*. 2017;12:7789–7797. doi:10.2147/IJN.S136748
24. Wang ZH, Tang M. Research progress on toxicity, function, and mechanism of metal oxide nanoparticles on vascular endothelial cells. *J Appl Toxicol*. 2021;41(5):683–700. doi:10.1002/jat.4121
25. Monsé C, Hagemeyer O, Raulf M, et al. Concentration-dependent systemic response after inhalation of nano-sized zinc oxide particles in human volunteers. *Part Fibre Toxicol*. 2018;15(1):8. doi:10.1186/s12989-018-0246-4
26. Holland NA, Becak DP, Shannahan JH, et al. Cardiac ischemia reperfusion injury following instillation of 20 nm citrate-capped nanosilver. *J Nanomed Nanotechnol*. 2015;6(S6):006. doi:10.4172/2157-7439.S6-006
27. Kolodziejczyk A, Jakubowska A, Kucinska M, et al. Sensing of silver nanoparticles on/in endothelial cells using atomic force spectroscopy. *J Mol Recognit*. 2018;31(9):e2723. doi:10.1002/jmr.2723
28. Jiang XM, Miclăuş T, Wang LM, et al. Fast intracellular dissolution and persistent cellular uptake of silver nanoparticles in CHO-K1 cells: implication for cytotoxicity. *Nanotoxicology*. 2015;9(2):181–189. doi:10.3109/17435390.2014.907457
29. Patlolla AK, Hackett D, Tchounwou PB. Silver nanoparticle-induced oxidative stress-dependent toxicity in sprague-dawley rats. *Mol Cell Biochem*. 2015;399(1–2):257–268. doi:10.1007/s11010-014-2252-7
30. Maurer LL, Meyer JN. A systematic review of evidence for silver nanoparticle-induced mitochondrial toxicity. *Environ Sci*. 2016;3(2):311–322.
31. Sun X, Yang Y, Shi JP, et al. NOX4- and Nrf2-mediated oxidative stress induced by silver nanoparticles in vascular endothelial cells. *J Appl Toxicol*. 2017;37(12):1428–1437. doi:10.1002/jat.3511
32. He J, Ma Y, Niu X, et al. Silver nanoparticles induce endothelial cytotoxicity through ROS-mediated mitochondria-lysosome damage and autophagy perturbation: the protective role of N-acetylcysteine. *Toxicology*. 2024;502:153734. doi:10.1016/j.tox.2024.153734
33. Khan I, Bahuguna A, Krishnan M, et al. The effect of biogenic manufactured silver nanoparticles on human endothelial cells and zebrafish model. *Sci Total Environ*. 2019;679:365–377. doi:10.1016/j.scitotenv.2019.05.045
34. Sinha K, Das J, Pal PB, et al. Oxidative stress: the mitochondria-dependent and mitochondria-independent pathways of apoptosis. *Arch Toxicol*. 2013;87(7):1157–1180. doi:10.1007/s00204-013-1034-4
35. Kim B, Song YS. Mitochondrial dynamics altered by oxidative stress in cancer. *Free Radic Res*. 2016;50(10):1065–1070. doi:10.1080/10715762.2016.1210141
36. Brillo V, Chieregato L, Leanza L, et al. Mitochondrial dynamics, ROS, and cell signaling: a blended overview. *Life*. 2021;11(4):332. doi:10.3390/life11040332
37. Zorov DB, Vorobjev IA, Popkov VA, et al. Lessons from the discovery of mitochondrial fragmentation (fission): a review and update. *Cells*. 2019;8(2):175. doi:10.3390/cells8020175